Technical Memorandum

MZA Associates Corporation

31 Mar 2006

To: WaveTrain users and developers

From: Boris Venet, MZA Associates (venet@mza.com, 505-245-9970)

Re: Validation of PartiallyCoherentReflector model in WaveTrain

Abstract

Speckle statistics for polychromatic light scattered from an optically rough reflector differ from the familiar exponential irradiance statistics found in monochromatic speckle. We derive an analytic result for the polychromatic speckle irradiance contrast for a simple reflector geometry, as a function of the geometry parameters and the coherence or spectral density parameters of the incident light. We then use this result to set up a quantitative test of WaveTrain's "PartiallyCoherentReflector" module, whose purpose is to numerically simulate the behavior of polychromatic (narrow-band) light scattered from an optically rough reflector.

Validation of "PartiallyCoherentReflector" model in WaveTrain

Boris Venet, MZA Associates

31 Mar 2006

1 Introduction

The purpose of WaveTrain's "PartiallyCoherentReflector" (PCR) module is to numerically simulate the reflection of light from an optically rough surface, when the incident light has a finite longitudinal (temporal) coherence, or equivalently put, is polychromatic to a certain extent. It is desired with the PCR numerical model to accurately simulate the propagation and speckle behavior when the longitudinal coherence varies over the domain from a few object macroscopic depths to a relatively small fraction of the macro-depth. The most obvious qualitative effect of the finite coherence is to reduce the contrast of the rough-surface speckle observed in a receiver plane. The reduction occurs because reflector points that are separated in macro-depth by more than the longitudinal coherence length will no longer produce stable interference: rather, the irradiances due to those reflector points will simply add.

Qualitatively, previous exercise of the PCR model showed that it certainly decreased speckle contrast, but the results had never been checked in any quantitative sense, specifically by comparison with analytically-derived results for a tractable geometry. There are several questions that need exploration as far as the numerical simulation model is concerned. Two key questions are: (a) Does the PCR simulation model actually give quantitatively correct speckle behavior for different combinations of target geometry and coherence? (b) How many "speckle realizations" are necessary to make the simulation model approach the correct statistics for given geometry/coherence parameters?

The present paper has the following purposes:

(a) We derive an analytic result for the speckle irradiance contrast for a simple reflector geometry, as a function of the geometry parameters and the coherence or spectral density parameters of the incident light.

(b) We review the concept used by WaveTrain's PCR numerical model.

(c) Using the results from (a), we set up a test case for checking the operation of the PCR wave-optics simulation model.

2 Theoretical speckle contrast for a test case

2.1 Geometry and monochromatic irradiance

Consider the geometry shown in Figure 1. Let the z axis be the nominal direction of the incident illumination, and let $\vec{\rho} = (x, y)$ be the transverse coordinate. The incident beam is scattered by an optically rough surface, which has an arbitrary orientation with respect to the axes. Let the plane $z = Z$ be a reference plane from which the surface depth function $d(\vec{\rho})$ is measured. This depth function refers only to the macroscopic surface shape, while the extra perturbation $h(\vec{\rho})$, a random process, designates the surface micro-roughness. We will begin with a spatially discrete model, using a single subscript to designate the two-dimensional grid point location. We will use the equivalent notations $d(\vec{\rho}_m) = d_m$, $h(\vec{\rho}_m) = h_m$, and so forth as is convenient. Let the plane $z = 0$ be the observation plane in which we want to compute speckle irradiance statistics. For single-point statistics it is sufficient to consider one observation point, P, which we place at the origin.

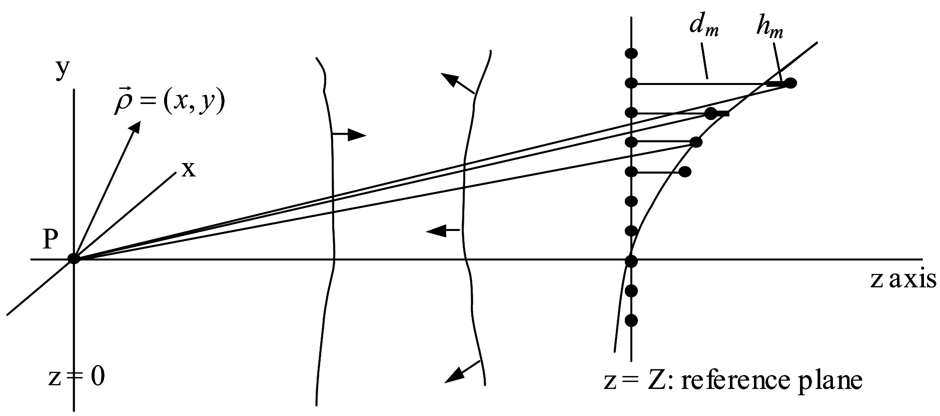

Figure 1: Scatter from an optically rough surface with depth profile

Our interest is in formulating the problem for polychromatic light, but we can build up that result by beginning with the more familiar monochromatic case. The key starting point is a formula for the net complex field at the observation point P. Using the discrete spot model of the surface, the net field at P can be expressed as the superposition of phasors that represent the phase lags from the reference plane to each discrete scatter point and then back to P. Let the incident complex field at $z = Z$ (monochromatic, with wave number $k = (2\pi)/\lambda$) be given by

$$\begin{aligned} V_m^0(k) &= A_m^0(k)\, e^{i\theta_m^0(k)}\; e^{-i(ck)t} \\ &= U_m^0(k)\, e^{-i(ck)t} \end{aligned} \tag{1}$$

The optical angular frequency factor written with $\omega = ck$ means that we assume dispersion is insignificant for our problem. (In purely monochromatic analysis, we typically drop the $\exp(-i\omega t)$ factor completely.) Now let R_m be the intensity reflectance, let ℓ_m be the physical path length from the reference plane to the scatter point and then to P, and let g be a geometry factor that represents the spread of the scattered light due to the back-propagation. With these definitions, the net complex field at P is

$$\begin{aligned} V(k) &= \left(\sum_{m=1}^{M} g\,\sqrt{R_m}\; e^{ik\ell_m}\, U_m^0(k) \right) e^{-ickt} \\ &= U(k)\, e^{-ickt} \end{aligned} \tag{2}$$

Equation (2) is a discrete version of the Fresnel-Kirchoff diffraction integral. We will also need an explicit decomposition for ℓ_m in terms of its several elements, namely

$$\begin{aligned} \ell_m &\approx d_m + h_m + \left(Z + d_m + h_m + \frac{\rho_m^2}{2Z} \right) \\ &= Z + 2d_m + 2h_m + \frac{\rho_m^2}{2Z} \end{aligned} \tag{3}$$

The quadratic approximation of Equation (3) is consistent with the usual Fresnel approximation.

Optical sensors are square-law devices that output a signal proportional to the time-average of the square of the electric field, where the averaging time is the response or integration time of the sensor. We will use the symbol $\overline{I}(k)$ to represent this irradiance. As shown in any general optics textbook, this time average for the monochromatic case turns out to be equivalent to the simple expression

$$\overline{I}(k) = U(k)\, U^*(k) \tag{4}$$

The only requirement for Equation (4) to hold is that

$$(integration\ time) >> 1/\,(optical\ \ frequency) \tag{5}$$.

2.2 Transition to the polychromatic case (finite bandwidth or finite longitudinal coherence)

The polychromatic field can be constructed from a Fourier superposition of monochromatic field terms defined in Equation (2):

$$V \;=\; \int dk\, V(k) \;=\; \int dk \sum_{m=1}^{M} g\sqrt{R_m}\; e^{i k \ell_m}\; U_m^0(k)\, e^{i c k t} \tag{6}$$

Next, we need an expression for the irradiance of the polychromatic field *V*. Computing this requires careful specification of the nature of the *k* dependence in $U_m^0(k)$. Unless one has a special known source model, one considers the polychromatic field amplitude to be a random process in the *k* space. To begin with, when we only deal with longitudinal coherence, it is useful to factor $U_m^0(k)$ as

$$U_m^0(k) = u_m^0 \cdot u^0(k) \tag{7}$$

where the $u^0(k)$ factor is a random process and the u_m^0 is a deterministic term that carries the space dependence. We assume that the deterministic factor u_m^0 is constant *over the spectral bandwidth*. The fact that the same $u^0(k)$ applies to all the space points is the meaning of finite *longitudinal* coherence. The factorization (7) yields

$$\begin{aligned} V &= \int dk\, u^0(k)\, e^{i c k t} \left[\sum_{m=1}^{M} g\sqrt{R_m}\, u_m^0\; e^{i k \ell_m} \right] \\ &= \int dk\, u^0(k)\, e^{i c k t} \left[\widetilde{U}(k) \right] \end{aligned} \tag{8}$$

where the second line defines the new symbol $\widetilde{U}(k)$.

We now skip a few derivation details and assert that the irradiance of the *V* field, under a certain condition on the optical bandwidth, is given by

$$\overline{I} = \int dk \; S(k)\, \widetilde{U}(k)\, \widetilde{U}^*(k) \qquad \text{where} \quad S(k) = \overline{u^0(k)\, u^{0^*}(k)} \tag{9}$$

The function *S* is called the spectral density, and the time-average overbar can alternately be viewed as an ensemble expectation value with respect to the ensemble of possible realizations of the spectral random process. The key condition that leads to Equation (9) is that

$$(integration\ time) >> 1/\,(frequency\ bandwidth\ of\ S) \tag{10}$$

The above mathematical model for polychromatic speckle follows the basic formulation given by Parry [(1)].

To reduce the future formula burden somewhat, we note that there is no loss of generality if we assume that *S* is normalized so that

$$\int dk \; S(k) = 1 \tag{11}$$

In the cases of interest to us, $S(k)$ is a relatively narrow function concentrated around some k_{avg}.

2.3 Spatial moments of the irradiance

It is important to note that Equation (9) for the polychromatic irradiance $\overline{I}$ has taken care of one random process present in the *V* field, namely the random fluctuations in magnitude and/or phase of the source field. We are assuming, because of condition (10), that $\overline{I}$ will *not* experience any noticeable temporal fluctuations due to the source random process (on the measurement time scale). There remains, however, another random process in $\overline{I}$, namely the h_m contained in the ℓ_m terms. A given realization of the h_m process produces a given, temporally fixed, spatial distribution of $\overline{I}$ in the observation plane: this is one realization of the polychromatic speckle. Different realizations of h_m would produce different distributions of $\overline{I}$ across the observation plane. We wish to compute a 1-point statistic, namely the spatial variance of the irradiance. We will compute this from the ensemble moments

$$\left\langle \overline{I} \right\rangle_h \quad \text{and} \quad \left\langle \overline{I}^2 \right\rangle_h \tag{12}$$

where the subscript emphasizes that this expectation value is with respect to the surface height random process only. The final quantity of interest is actually the normalized irradiance variance (*NIV*), that is, [variance / mean^2]. Alternatively, the "contrast" is usually defined as [standard deviation / mean] = $\sqrt{NIV}$. Once we have $\left\langle \overline{I} \right\rangle_h$ and $\left\langle \overline{I}^2 \right\rangle_h$, we can easily combine these to form the *NIV* or contrast.

[1] Parry, G.: "Speckle Patterns in Partially Coherent Light", in *Laser Speckle and Related Phenomena*, *2nd ed.*, J.C. Dainty (ed.), pp. 77 ff., Springer-Verlag, 1984.

We said above that $\overline{I}$ has no measurable temporal fluctuations due to the source phase random process. However, the width of the spectral density will still affect the calculation of the second spatial moment of $\overline{I}$. Qualitatively this comes about because Equation (9), for any given height realization, adds speckle irradiances corresponding to different wave numbers and these patterns are slightly displaced from one another and therefore smear the monochromatic contrast.

2.4 Evaluation of $\left\langle \overline{I} \right\rangle_h$

Combining Equations (9), (8) and (3), we have

$$\begin{aligned} \left\langle \overline{I} \right\rangle_h &= \left\langle \int dk\; S(k)\, \widetilde{U}(k)\, \widetilde{U}^*(k) \right\rangle_h \\ &= \int dk\; S(k)\, g^2 \sum_{m,n} \sqrt{R_m}\, \sqrt{R_n}\, u_m^0\, u_n^{0^*}\; e^{i2k\left(d_m - d_n + \frac{\rho_m^2 - \rho_n^2}{4Z} \right)} \left\langle e^{i2k(h_m - h_n)} \right\rangle \end{aligned} \tag{13}$$

We can evaluate the expectation value factor containing the surface heights, if we assume that the heights are Gaussian, independent, identically distributed random variables. This is the typical assumption made in the scatter spot model for speckle. In that case, the expectation value becomes

$$\left\langle e^{i2k(h_m - h_n)} \right\rangle = \begin{cases} e^{i2k\langle (h_m - h_n) \rangle}\; e^{-\frac{1}{2} 4k^2 \sigma^2 (h_m - h_n)} = e^{-4k^2 \sigma_h^2} & , \quad m \neq n \\ 1 \quad , \quad m = n \end{cases} \tag{14}$$

where σ_h^2 is the surface height variance. (The basic result for <exp(*i**Gaussian)> is given, for example, in Goodman [2]).

The factor $\exp\left(-4k^2 \sigma_h^2\right)$ can be rewritten as $\exp\left(-16\pi^2 \cdot (\sigma_h/\lambda)^2\right)$. So, if the surface height standard deviation is of order 1 wavelength or more, the exp(…) factor is of order $e^{-160} \approx 3 \cdot 10^{-70}$ or less. Substituting Equation (14) into Equation (13) yields a result comprising two classes of terms, corresponding to the two sums in the following equation:

$$\begin{aligned} \left\langle \overline{I} \right\rangle_h = g^2 \int dk\; S(k) \Bigg\{ &\sum_m R_m \left| u_m^0 \right|^2 \\ &+ e^{-4k^2 \sigma_h^2} \sum_{m \neq n} \sqrt{R_m}\, \sqrt{R_n}\, u_m^0\, u_n^{0^*}\; e^{i2k\left(d_m - d_n + \frac{\rho_m^2 - \rho_n^2}{4Z} \right)} \Bigg\} \end{aligned} \tag{15}$$

Using the fact that $\left| x_1 + \ldots + x_M \right| \leq \left| x_1 \right| + \cdots + \left| x_M \right|$ and that $\exp\left(-4k^2 \sigma_h^2\right)$ is miniscule as discussed above, we can neglect the second term in Equation (15) compared to the first (even though the second term contains $M(M-1)$ summands, compared to the first term's M summands). Thus, $\left\langle \overline{I} \right\rangle_h$ reduces to

[2] J.W. Goodman, Statistical Optics, p. 400, Wiley, 1985.

$$\left\langle \overline{I} \right\rangle_h = g^2 \int dk\, S(k) \sum_m R_m \left| u_m^0 \right|^2 \\ = g^2 \sum_m R_m \left| u_m^0 \right|^2 \tag{16}$$

To obtain the second line of Equation (16), we used two facts: $\left| u_m^0 \right|^2$ changes negligibly over the spectral bandwidth, and S is normalized according to Equation (11). Contemplating the result (16), it may now seem obvious from the standpoint of energy conservation. We went through the trouble of showing the intermediate steps because manipulations of the same general type, but with more algebraic complications, will be used to obtain the second moment $\left\langle \overline{I}^2 \right\rangle_h$.

2.5 Evaluation of $\left\langle \overline{I}^2 \right\rangle_h$

Again using Equations (9), (8) and (3), we have

$$\begin{aligned} \left\langle \overline{I}^2 \right\rangle_h &= \left\langle \int dk_1\, S(k_1)\, \widetilde{U}(k_1)\, \widetilde{U}^*(k_1) \cdot \int dk_2\, S(k_2)\, \widetilde{U}(k_2)\, \widetilde{U}^*(k_2) \right\rangle \\ &= \int dk_1 \int dk_2\, S(k_1) S(k_2) \left\{ g^4 \sum_{m,n,p,q} \sqrt{R_m}\, \sqrt{R_n}\, \sqrt{R_p}\, \sqrt{R_q}\; u_m^0\, u_n^{0^*}\, u_p^0\, u_q^{0^*} \right. \\ &\qquad \left. \cdot\, e^{i2\left[k_1 \left(d_m - d_n + \frac{\rho_m^2 - \rho_n^2}{4Z} \right) + k_2 \left(d_p - d_q + \frac{\rho_p^2 - \rho_q^2}{4Z} \right) \right]} \left\langle e^{i2\left[k_1 (h_m - h_n) + k_2 (h_p - h_q) \right]} \right\rangle \right\} \end{aligned} \tag{17}$$

Using the same concepts employed earlier, we can evaluate the exponential expectation value (i.e., the last factor) in Equation (17). Defining $\phi = k_1 (h_m - h_n) + k_2 (h_p - h_q)$, we have

$$\left\langle e^{i2\phi} \right\rangle = e^{i2\langle \phi \rangle}\, e^{-\frac{1}{2}\cdot 4\sigma_\phi^2} \tag{18}$$

The heights are assumed zero-mean and identically distributed. Therefore the first factor in Equation (18) is simply 1, while in the second factor the variance of ϕ reduces to

$$\sigma_\phi^2 = k_1^2 \left\langle h_m^2 + h_n^2 - 2h_m h_n \right\rangle + k_2^2 \left\langle h_p^2 + h_q^2 - 2h_p h_q \right\rangle + 2\, k_1 k_2 \left\langle h_m h_p - h_n h_p - h_m h_q + h_n h_q \right\rangle \tag{19}$$

Writing

$$\left\langle h_j^2 \right\rangle = \sigma_h^2 \;\text{ for all } j, \;\text{ and } \left\langle h_m h_n \right\rangle = \delta_{mn}\, \sigma_h^2$$

where δ_{mn} is Kronecker's delta, Equation (19) can be conveniently rewritten as

$$\sigma_\phi^2 = 2\sigma_h^2 \cdot \left\{ k_1^2 \left(1 - \delta_{mn} \right) + k_2^2 \left(1 - \delta_{pq} \right) + k_1\, k_2 \left(\delta_{mp} - \delta_{np} - \delta_{mq} + \delta_{nq} \right) \right\} \tag{20}$$

Consider now various possible cases of equality and inequality among $\{m, n, p, q\}$. The various Kronecker deltas always take on the values 0 or 1. The following list shows three particular combinations:

$$m = n \text{ and } p = q: \quad \sigma_\phi^2 = 0 \;, \quad \text{and } e^{-2\sigma_\phi^2} = 1 \tag{21}$$

$$m = q \text{ and } n = p, \text{ but } m \neq n: \quad \sigma_\phi^2 = 2\sigma_h^2 (k_1 - k_2)^2 \;, \quad \text{and } e^{-2\sigma_\phi^2} = e^{-4\sigma_h^2 (k_1-k_2)^2} \tag{22}$$

$$m \neq n \text{ and } p = q: \quad \sigma_\phi^2 = 2\sigma_h^2 k_1^2 \;, \quad \text{and } e^{-2\sigma_\phi^2} = e^{-4\sigma_h^2 k_1^2} \tag{23}$$

The exponential factor at the far right of the preceding equations is what appears in Equation (18) and hence in the terms of the master Equation (17). We have met the exponential factor of case (23) before, when we evaluated $\langle \bar{I} \rangle_h$ and we noted its miniscule size (recall Equation (14) and the subsequent discussion). Careful examination of all other subscript equality-inequality cases shows that all the cases not shown in the above list have the general character of case (23). Therefore, the only two terms that may substantially contribute to Equation (17) are cases (21) and (22).

Using the results of the previous paragraph, Equation (17) reduces to

$$\begin{aligned} \left\langle \bar{I}^2 \right\rangle_h = \int dk_1 \int dk_2\, S(k_1) S(k_2) \Bigg\{ & g^4 \sum_{m,p} R_m R_p \left| u_m^0 \right|^2 \left| u_p^0 \right|^2 \\ & + g^4 \sum_{m,n} R_m R_n \left| u_m^0 \right|^2 \left| u_n^0 \right|^2 e^{i2(k_1-k_2)\left(d_m - d_n + \frac{\rho_m^2 - \rho_n^2}{4Z}\right)} e^{-4\sigma_h^2 (k_1-k_2)^2} \Bigg\} \end{aligned} \tag{24}$$

$$\equiv T1 + T2$$

Inspection of Equation (16) shows that the first term of Equation (24), $T1$, is simply

$$T1 = \left\langle \bar{I} \right\rangle_h^2 \tag{25}$$

To evaluate $T2$, we carry out the wave number integrations first. Since the integrand depends only on ($k_1 - k_2$), we change integration variables from (k_1, k_2) to sum and difference coordinates ($K = (k_1 + k_2)/2$, $\kappa = k_1 - k_2$). Making the change of variables and then doing the K integral first yields

$$\begin{aligned} T2k &\equiv \int dk_1 \int dk_2\, S(k_1) S(k_2)\, e^{i2(k_1-k_2)\left(d_m - d_n + \frac{\rho_m^2 - \rho_n^2}{4Z}\right)} e^{-4\sigma_h^2 (k_1-k_2)^2} \\ &= \int d\kappa \left[\int dK\; S(K + \tfrac{1}{2}\kappa) S(K - \tfrac{1}{2}\kappa) \right] e^{i2\kappa\left(d_m - d_n + \frac{\rho_m^2 - \rho_n^2}{4Z}\right)} e^{-4\sigma_h^2 \kappa^2} \\ &= \int d\kappa \left(B_S(\kappa)\, e^{-4\sigma_h^2 \kappa^2} \right) e^{i2\kappa\left(d_m - d_n + \frac{\rho_m^2 - \rho_n^2}{4Z}\right)} \end{aligned} \tag{26}$$

The new symbol $B_S(\kappa)$ in the last line of Equation (26) is the deterministic autocorrelation of $S(k)$, which appeared in the square brackets of the preceding line. Note also that the last line of Equation (26) can be interpreted as an inverse Fourier transform, evaluated at the space variable $\xi_{m,n}$, where $\xi_{m,n} = 2\left(d_m - d_n + (\rho_m^2 - \rho_n^2)/4Z\right)$. That is, it may be helpful to write

$$T2k = \mathbf{F}_\kappa^{-1}\left\{ B_S(\kappa)\, e^{-4\sigma_h^2 \kappa^2} \right\}\Bigg|_{\xi_{m,n}} \tag{27}$$

The full $T2$ term of Equation (24) is therefore

$$T2 = g^4 \sum_{m,n} R_m R_n \left|u_m^0\right|^2 \left|u_n^0\right|^2 \mathbf{F}_\kappa^{-1}\left\{ B_S(\kappa)\, e^{-4\sigma_h^2 \kappa^2} \right\}\Bigg|_{\xi_{m,n}} \tag{28}$$

It is important to realize that the exponential factor $\exp\left(-4\kappa^2\sigma_h^2\right)$ in Equation (28) is a very different animal than the previously encountered factor $\exp\left(-4k^2\sigma_h^2\right)$, which we argued was negligible. The reason is that κ is a *difference* wavenumber, which ranges over only a small increment around 0, whereas k was a wave number ranging over an increment around the average optical wave number.

2.6 NIV

Finally we can obtain our end goal, the speckle NIV, by combining the Equations (25) and (28) for $T1$ and $T2$:

$$\begin{aligned} NIV &= \frac{\left\langle \overline{I}^2 \right\rangle_h - \left\langle \overline{I} \right\rangle_h^2}{\left\langle \overline{I} \right\rangle_h^2} = \frac{(T1+T2)-T1}{T1} \\ &= \frac{\displaystyle\sum_{m,n} R_m R_n \left|u_m^0\right|^2 \left|u_n^0\right|^2 \mathbf{F}_\kappa^{-1}\left\{ B_S(\kappa)\, e^{-4\sigma_h^2 \kappa^2} \right\}\Bigg|_{\xi_{m,n}}}{\displaystyle\sum_{m,p} R_m R_p \left|u_m^0\right|^2 \left|u_p^0\right|^2} \end{aligned} \tag{29}$$

Formula (29) is almost as far as we can reduce the answer in general. To proceed much further and obtain numerical answers, we must specify explicit functional forms for the spectral density function, the incident spatial field dependence, and the reflectance spatial dependence. In the next section, we work out a numerical example that can be used for detailed testing of the WaveTrain PartiallyCoherentReflector module.

Before proceeding to a complete numerical example, there is actually one more approximation we can make that will frequently be very good, at least when the illuminator is a laser. The factor $\exp\left(-4\kappa^2\sigma_h^2\right)$ in Equation (29) will often be very nearly equal to 1, over the entire κ domain for which the spectral density (and hence the autocorrelation $B_S(\kappa)$) is non-negligible. To see this, we write

$$4\left(\kappa_{\max}\,\sigma_h\right)^2 = 4\left((\Delta k)_{\max}\cdot\sigma_h\right)^2 \approx 4\left(2\pi\frac{(\Delta f)_{\max}}{f_{avg}}\frac{\sigma_h}{\lambda_{avg}}\right)^2 = \left(4\pi\frac{(\Delta f)_{\max}}{f_{avg}}\frac{\sigma_h}{\lambda_{avg}}\right)^2 \tag{30}$$

Evidently, if

$$\frac{(\Delta f)_{\max}}{f_{avg}} << 1 \Bigg/ \left(4\pi \frac{\sigma_h}{\lambda_{avg}} \right) \tag{31}$$

then $\exp\left(-4\kappa^2\sigma_h^2\right) \approx 1$. Table 1 shows some examples that indicate this relation will frequently be satisfied. The table assumes $\lambda_{avg} = 1\mu m$ and correspondingly $f_{avg} = 3 \cdot 10^{14}\, Hz$:

$\frac{(\Delta f)_{\max}}{f_{avg}}$	$1 \Big/ \left(4\pi \frac{\sigma_h}{\lambda_{avg}} \right)$
1GHz / 3E14Hz = 3E-6	$1/(4\pi \cdot 1)$ = 8E-2
	$1/(4\pi \cdot 100)$ = 8E-4
1MHz / 3E14Hz = 3E-9	$1/(4\pi \cdot 1)$ = 8E-2
	$1/(4\pi \cdot 100)$ = 8E-4

Table 1: Numerical examples related to Equation (31)

From the tabulated examples, it seems that inequality (31) will typically be satisfied for laser illumination. When the inequality is satisfied, the *NIV* result (29) simplifies further to

$$NIV = \frac{\sum\limits_{m,n} R_m\, R_n \left|u_m^0\right|^2 \left|u_n^0\right|^2 \mathbf{F}_\kappa^{-1}\left\{B_S(\kappa)\right\}\Big|_{\xi_{m,n}}}{\sum\limits_{m,p} R_m\, R_p \left|u_m^0\right|^2 \left|u_p^0\right|^2} \tag{32}$$

2.7 *NIV* evaluated numerically for specific functional forms

Consider the following example:

- The reflector is a rectangular plate with dimensions $L_1 \times L_2$. The L_1 edges are parallel to the *x* axis, and the L_2 edges are tilted at angle θ with respect to the *y* axis (see Figure 2). Therefore, the mean depth function of the plate is $d_m = y_m \tan\theta$. The total depth of the plate is $L_z = L_2 \sin\theta$, and the projected *y*-width is $L_y = L_2 \cos\theta$, as sketched below.

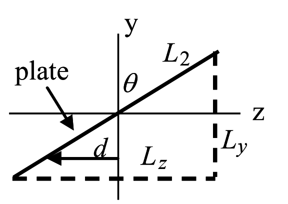

Figure 2: Tilted rectangular plate geometry

- The reflectance is uniform.
- The spatial dependence of the incident field is a plane wave with wave vector along *z*.
- The spectral density function has a Gaussian shape, given by

$$S(\kappa) = \sqrt{\frac{2}{\pi D_\kappa^2}}\, e^{-2\left(\frac{\kappa}{D_\kappa}\right)^2} \tag{33}$$

Note the bandwidth D_κ is defined as the 1/e^2 half-width, and $S(\kappa)$ is area-normalized to 1.

- The bandwidth D_κ satisfies Equation (31), so that *NIV* is given by Equation (32).

Evaluation of the spectral autocorrelation and Fourier transform required by the *NIV* formula yields

$$\mathbf{F}_\kappa^{-1}\left\{B_S(\kappa)\right\}\Big|_{\xi_{m,n}} = e^{-\left[D_\kappa\left(d_m - d_n + \frac{\rho_m^2 - \rho_n^2}{4Z}\right)\right]^2} \tag{34}$$

Finally, we substitute this into Equation (32) and compute the remaining sums. When we derived Equation (32) it was convenient to use a spatially discrete model for the random surface (Goodman's "scatter-spot" model). But, at the present stage it is more convenient to transition to a continuum model. This means replacing each sum in Equation (32) by an area integral. It is convenient to express the support domain of the reflectance factors by using the rectangle function $\mathrm{rect}(t) = \left\{1 \text{ if } |t| \le \frac{1}{2},\, 0 \text{ otherwise}\right\}$. The numerator of Equation (32) then becomes

$$num_{NIV} = R^2 \left|u^0\right|^4 \left\{\int d^2\rho\, \mathrm{rect}\!\left(\frac{x}{L_1}\right) \mathrm{rect}\!\left(\frac{y}{L_y}\right) \int d^2\rho'\, \mathrm{rect}\!\left(\frac{x'}{L_1}\right) \mathrm{rect}\!\left(\frac{y'}{L_y}\right) \cdot e^{-\left[D_\kappa\left((y-y')\tan\theta + \frac{x^2+y^2-x'^2-y'^2}{4Z}\right)\right]^2}\right\} \tag{35}$$

Now we make a final approximation: except for plate tilts $\theta \approx 0$, the quadratic terms in the *real* exponential of the preceding integral are completely negligible compared to the linear terms. In that case, the *x* integrals become trivial, and the *y* integrals can be simplified by changing to sum and difference coordinates. The final result is the simple expression

$$NIV = \frac{num_{NIV}}{den_{NIV}} = \int dt\, \mathrm{tri}(t) \cdot e^{-\left(D_k L_z t\right)^2} \tag{36}$$

where the triangle function $\mathrm{tri}(t)$ is 1 at $t = 0$ and drops linearly to 0 at $t = \pm 1$. This final integral must be evaluated numerically, and the result is shown as the red solid curve in Figure 3.

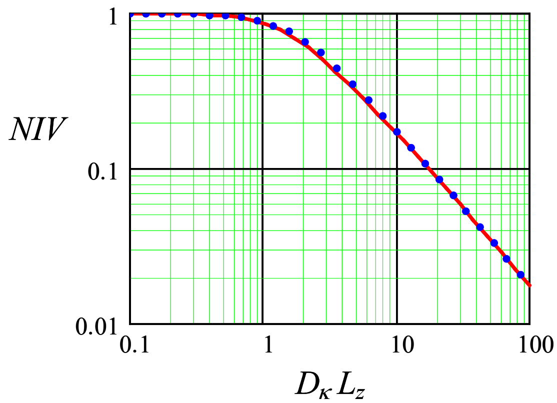

Figure 3: Speckle *NIV* for the tilted rectangular plate, when illumination has finite bandwidth

The *NIV* depends only on the product parameter $D_\kappa L_z$, where L_z is simply the total depth of the plate (the actual length and tilt only enter as the combination $L_z = L_2 \sin\theta$). Recall also that *NIV* is actually not exactly 1 when $L_z = 0$, since we have neglected the quadratic terms in Equation (35). When $D_\kappa L_z$ is large enough, the Gaussian factor in Equation (36) is very narrow compared to the triangle factor. In that asymptotic case, the integral can be evaluated analytically, and we find that $NIV \approx \sqrt{\pi}/(D_k L_z)$. Smoothly merging the two asymptotes with an empirical joining function, we can obtain a simple semi-empirical formula that accurately represents the computed results over the whole domain (see the dots in Figure 3):

$$NIV \approx \left[1 + \left(\frac{1}{\sqrt{\pi}} D_\kappa L_z\right)^2\right]^{-1/2} \tag{37}$$

Notice that *NIV* decreases quite slowly, proportional to $(D_\kappa L_z)^{-1}$. The contrast decreases even more slowly, proportional to $(D_\kappa L_z)^{-1/2}$.

To see what the *NIV* or contrast numbers are for a few laser bandwidths, consider sources with bandwidths of $D_f = 10\ MHz$ and $10\ GHz$, and let $L_z = 1\ m$. Since $k = (2\pi f)/c$, the differential implies $D_\kappa = (2\pi/c) D_f$, that is $D_\kappa = 0.21\ rad/m$ and $210\ rad/m$ for the two cases. From Figure 3 or Equation (37), the *NIV* for the two cases is 0.993 and 0.0084, while the contrast is 0.996 and 0.092 .

2.7.1 Coherence length

Since the wave number superposition was fundamental in the theoretical analysis, the spectral density width D_κ was a natural width measure to use in our development of the *NIV* result. But there is another bandwidth measure that frequently arises in experimental practice, namely the "coherence length", ℓ_{coh}, of the illuminator. Coherence length is typically measured via fringe visibility in a Michelson interferometer setup. The coherence length is defined as the path-length difference that reduces fringe visibility from 1 to some specified level. Since coherence length in this sense is frequently used or specified to characterize sources, it is important to relate this quantitatively to the D_κ width measure. It can be shown that the fringe visibility as a function of path length difference is the Fourier transform of the spectral density function.

Therefore, for the Gaussian spectral density in our numerical example, i.e., Equation (33), the visibility function is also Gaussian, and the 1/e^2 coherence length is related to D_κ (which was also a 1/e^2 width) by the exact relation

$$\ell_{coh} = \frac{4}{D_\kappa} \tag{38}$$

With this result for coherence length, we can rewrite Equation (37) as

$$NIV \approx \left[1 + \left(\frac{4}{\sqrt{\pi}}\frac{L_z}{\ell_{coh}}\right)^2\right]^{-1/2} \tag{39}$$

When $L_z/\ell_{coh} >> 1$, $NIV \to \left(\sqrt{\pi}/4\right)\cdot\left(\ell_{coh}/L_z\right)$. If we assume a qualitative model in which the scatter from successive "coherence depths" adds incoherently, then the proportionality $NIV \propto \left(\ell_{coh}/L_z\right)$ can be derived very simply from the addition of independent random variables. This provides a check on the rather complicated derivation leading to Equations (36) and (39)

From Equation (38), the two bandwidths $D_\kappa = 0.21\ rad/m$ and $210\ rad/m$ for which we computed *NIV* and contrast in the previous subsection correspond to $\ell_{coh} \approx 19\ m$ and $1.9\ cm$ respectively.

2.7.2 Cautionary comments

The precise numerical values of the breakpoints in the *NIV* Equations (37) and (39) depend on the assumption of Gaussian spectral density. For a different spectral shape, say a Lorentzian, these breakpoints will be somewhat different, although the asymptotic slopes are most likely the same. In practice, when a source is said to have a certain coherence length, it is often murky at best whether a 1/e^2 or ½ or some other visibility level is meant. With lasers, the situation is often also complicated by the fact that the shape of the visibility function is not an analytically simple form. In practice then, we expect the proportionality $NIV \propto \left(\ell_{coh}/L_z\right)$ indicated by Equation (39), but the exact proportionality factor will be in doubt.

3 Review of WaveTrain's "PartiallyCoherentReflector" numerical model

WaveTrain's PCR simulation model works directly with a space-time statistical representation of the partially coherent illumination. The simulation procedure does not exactly parallel the spectral superposition approach that we used in Section 2 to work out a theoretical *NIV*. However, the space-time approach should be equivalent: if we use corresponding spectral density functions or temporal correlation functions, then the simulation calculation should yield results identical to what we computed theoretically in Section 2.

WaveTrain's PCR model works as follows. Consider the sketch in Figure 4. The curved line represents an optically rough reflecting surface, which is illuminated by a wave traveling paraxially in the *z* direction. z_0 is a reference plane from which the macroscopic depth map, $d(x, y)$, of the target surface is specified. The micro-roughness of the surface, in the optical sense, is a spatially random fine-scale perturbation on top of the macroscopic *d* map.

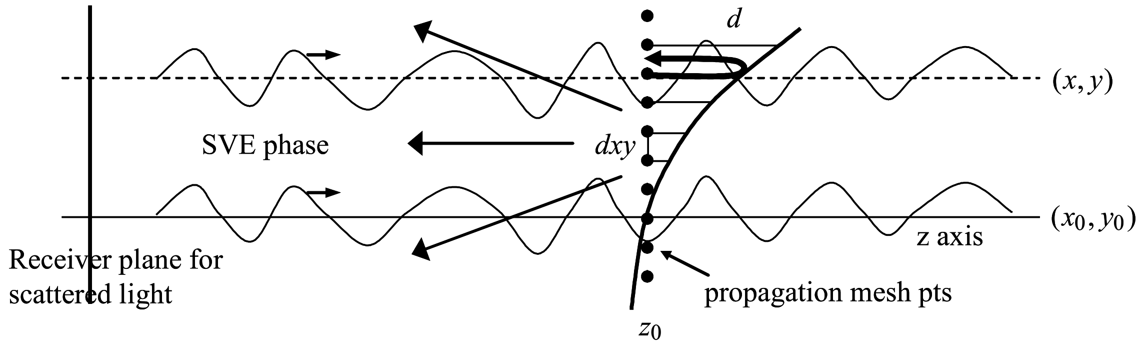

Figure 4: Simulation of rough-surface reflection with partial longitudinal coherence

The PCR concept is an elaboration of the method used to treat the scattering of completely coherent illumination. For completely coherent light (WaveTrain's "CoherentTarget" module), we represent the reflected complex field that exits the discrete mesh in the z_0 reference plane as

$$U_{i,j}^{rfl} = \sqrt{\alpha R_{i,j}}\; U_{i,j}^{inc}\, e^{i\delta_{i,j}} \tag{40}$$

where $U^{inc}(x_i, y_j)$ is the incident complex field, $\delta(x_i, y_j)$ is a spatially uncorrelated phase, $R(x_i, y_j)$ is an intensity reflectance map, and α is a radiometric normalization factor required because of our discrete Fourier Transform methods (the α factor is discussed in other documentation, and is not specifically a PCR property). The mod-2π values of δ are assumed for practical purposes to be uniformly distributed over (0, 2π□). This model [3, 4] is sometimes called the scatter-spot model. In this basic model, the deterministic depth map has no effect on the statistical properties of the scattered light recorded in the receiver plane, and is ignored in the formalism. Now consider a beam with finite longitudinal coherence. Most cases of interest are still "quasi-monochromatic", such that the slowly-varying envelope (SVE) representation is a useful mathematical device. The incident field is described by

$$\Psi(\vec{\rho}, z, t) = U(\vec{\rho}, z, t)\, e^{\,i(k_0 z - \omega_0 t)} \tag{41}$$

where $\vec{\rho} = (x, y)$, k_0 and ω_0 refer to the nominal optical wavelength λ_0, and U is the slowly-varying complex envelope factor. In general, WaveTrain operates only on the U factor, and does not keep track of the "carrier" phasor $e^{\,i(k_0 z - \omega_0 t)}$. In most WaveTrain operations, the t dependence of U arises only from turbulence and/or relative component motion. However, in the PCR model, we explicitly construct a space-time representation of the SVE envelope: this envelope is notionally pictured at one instant as the irregular wave in the Figure 4 sketch. The first key operation of the PCR model is to construct one instantaneous realization of the partially-coherent SVE envelope factor $A_S(z)\exp\left(i\phi_S(z)\right)$, assuming that we have a Gaussian random process with correlation length ℓ_{coh}, which is a user input of the model. The realization is

---

3 Frieden, , B.R.: *Probability, Statistical Optics, and Data Testing, 2nd ed.*, pp. 105 ff., Springer-Verlag, 1991.

4 Goodman, J.W.: "Statistical properties of laser speckle patterns", in *Laser Speckle and Related Phenomena*, J.C. Dainty (ed.), pp. 9 ff., Springer-Verlag, 1975.

constructed over a total length L_S, on a mesh with spacing dz_S. L_S is also a user input of the model. The next step is to construct one realization of the reflected complex field array, $U^{rfl}(x_i, y_j)$, exiting the discrete propagation mesh in the z_0 reference plane. By extension from Equation (40), we write

$$U_{i,j}^{rfl} = \sqrt{\alpha R_{i,j}}\; U_{i,j}^{inc}\; A_S(z_0 + 2d_{i,j})\; e^{i\phi_S(z_0+2d_{i,j})}\; e^{i\delta_{i,j}} \tag{42}$$

The realization $U_{i,j}^{rfl}$ is then propagated away from the z_0 plane towards the receiver using the same Fourier methods as for any completely coherent field. One such realization would give the same statistical properties (fully-developed speckle) at the receiver as the basic coherent-illumination (CoherentTarget) model described by Equation (40). To obtain the desired partially coherent result, we now repeat the propagation step with a sequence of N_w realizations of $U_{i,j}^{rfl}$. Each realization is obtained from Formula (42) by the replacement

$$A_S(z_0 + 2d_{i,j})\; e^{i\phi_S(z_0+2d_{i,j})} \quad\rightarrow\quad A_S(z_0 + n\cdot\Delta z_S + 2d_{i,j})\; e^{i\phi_S(z_0+n\cdot\Delta z_S+2d_{i,j})} \tag{43}$$

where $n = 0,\ldots,N_w - 1$, and $\Delta z_S = L_S / N_w$. $\{\ell_{coh}, L_S$, and $N_w\}$ are the three SVE-related user inputs of the PCR model. When the N_w realizations are propagated to the receiver plane, this procedure represents an actual temporal sequence of complex fields that a receiver would experience due to the SVE illumination. The temporal sequence of irradiance patterns at the receiver plane consists of speckle patterns that are somewhat shifted (and distorted) from one another. Finally, the PCR model assumes that the response time of the sensor is slow enough so that only the average irradiance over the N_w realizations is reported by the sensor. If N_w sufficiently samples all the correlation lengths contained within the target macro-depth L_z, then this discretely-computed average should exhibit the speckle contrast reduction appropriate to the specified combination of coherence length and target macro-depth.

Figure 5 may help to clarify the required combination of parameters that provides sufficient sampling for validity of the PCR algorithm. The key parameters in question are the SVE-related input parameters $\{\ell_{coh}, L_S$, and $N_w\}$. The curved line in Figure 5, with known total depth L_z, represents the rough reflecting surface.

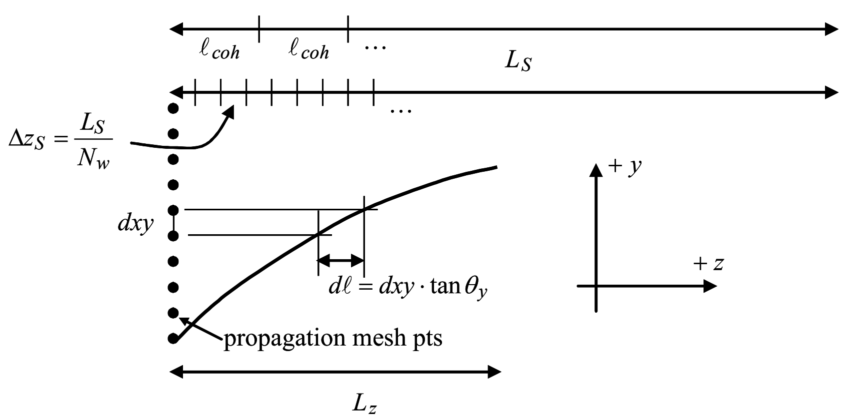

Figure 5: Choosing consistent parameters for the WaveTrain PCR model

The distance L_S is the length (in meters) of the space-time realization of the SVE random process. This realization is generated by an algorithm that produced a periodic realization, so we recommend setting L_S = $2\,L_z$. If we sample the SVE envelope at least several times per correlation length, we should sufficiently resolve that variation to model any variations in the resulting speckle pattern. We express this requirement as

$$\frac{L_S}{N_w} < \frac{\ell_{coh}}{several} \quad \Rightarrow \quad N_w > (several)\frac{L_S}{\ell_{coh}} \tag{44}$$

Next, consider the distance labeled $d\ell$ in Figure 5. This depth increment corresponds to the projection of the propagation mesh spacing dxy onto the reflecting surface, where θ_y is the local inclination of the surface with respect to the y-axis. The sketch shows a y-z projection, but there is an analogous projection for x-z. Again, in order for the numerical procedure to sample the SVE correlation length interacting with the surface, we should have $d\ell$ less than some fraction of ℓ_{coh}. We express this requirement as

$$d\ell < \frac{\ell_{coh}}{several} \quad \Rightarrow \quad dxy < \frac{\ell_{coh}}{(several)\cdot \tan\theta_{x,y}} \tag{45}$$

In sum, given { L_z , L_S and ℓ_{coh} }, inequality (44) guides us in selecting the remaining SVE parameter N_W. Inequality (45) can be viewed as a constraint on the propagation mesh, or on the inclination of the target that can be accurately modeled. For a complex target, $\tan\theta_{x,y}$ will be a complicated variable quantity, and it may not be necessary to satisfy inequality (45) everywhere, as long as the violating areas return insignificant power. At this point, there is some lack of precision about the constraints (44) and (45), due to the "(several)" factor and the potential complexity of $\tan\theta_{x,y}$.

4 Comparison of theory with a numerical simulation using WaveTrain's "PartiallyCoherentReflector" model

The case of the tilted rectangular plate and Gaussian spectral density, for which we worked out numerical details from theory in Section 2.7, can be set up in WaveTrain as a test of the PartiallyCoherentReflector (PCR) module.

Let us choose the following WaveTrain propagation parameters for our PCR test system:

- 0 turbulence, $\lambda = 1\ \mu m$, $Z = 50\ km$, propagation grid dimension $N = 256$ points, grid spacing $dx = \sqrt{\lambda z/N} = 1.40\ cm$ (Fresnel criterion), grid width $N \cdot dx = 3.58\ m$
- Reflector square of size $L \times L = 1m \times 1m$, inclined from y-axis at θ=0, 10, 30, and 80 *deg* (see Figure 2). This is implemented with two types of PCR input maps (WaveTrain "Grids"):
  (a) A depth map for each θ: $d_{i,j} = y_j \cdot \tan\theta$, where (i, j) span $(L\ , L\cos\theta)$.
  (b) A reflectance map for each θ: $R_{i,j} = 1.0$, where (i, j) span $(L\ , L\cos\theta)$.
- The PCR module has an input parameter called "coherenceLength". This coherence length is a $1/e^2$ length, where the visibility (or correlation) function is Gaussian. Therefore, the PCR "coherenceLength" should correspond precisely to ℓ_{coh} as defined in the preceding theoretically-based numerical example.

If we let ℓ_{coh} = 0.50, 0.10, 0.02 *m*, then Equation (39) tells us that the specified combination of ℓ_{coh} and θ parameters should correspond to the range of *NIV* tabulated in Table 2. Notice that the range of speckle contrast that we obtain from the parameter domain in the table is only one order of magnitude, while the range of *NIV* is two orders of magnitude.

			NIV **(*Contrast*)**		
θ (deg)	$L_z = L\sin\theta$ (m)	$L_y = L\cos\theta$ (m)	ℓ_{coh} = 0.50 m	ℓ_{coh} = 0.10 m	ℓ_{coh} = 0.02 m
0	0	1	1 **(1)**	1 **(1)**	1 **(1)**
10	0.174	0.985	0.77 **(0.88)**	0.23 **(0.48)**	0.051 **(0.23)**
30	0.500	0.866	0.38 **(0.62)**	0.089 **(0.30)**	0.018 **(0.13)**
80	0.985	0.174	0.21 **(0.46)**	0.045 **(0.21)**	0.0090 **(0.095)**

Table 2: Expected range of speckle *NIV* spanned by the WaveTrain test inputs

- The final key input parameter in the PCR module is "nWaves". This is the parameter denoted N_w in the conceptual overview Section 3. We performed test runs for N_w = 20 and 100. In the discussion of results below, we will relate these values to the inequality requirements discussed at the end of Section 3.

- Sensor parameters in the WaveTrain receiver plane:
We want to compute the speckle irradiance in the simulated observation plane for each combination of the test parameters. To make a valid comparison between theory and simulation, we must bear in mind several artifacts that arise in the simulated Fourier transform propagation on a discrete, finite mesh.
(i) The first item to consider is peculiar to the case of propagation from an optically rough source plane, where the transverse phase has a spatially uncorrelated term distributed over (0, 2π). In a physical experiment this light would have a wide divergence, but on the discrete Fourier transform mesh the light from each mesh point only diverges by an amount limited by the propagation mesh spacing, as sketched in Figure 6. The consequence is that the scattering model is only valid in the overlap region indicated in Figure 6 by the segment labeled L_{uni}: in this region, all discrete source points that comprise the specified reflector contribute to the net light field, as they would in a physical experiment. When we compute the speckle statistics, we must limit ourselves to a region of interest (ROI) in the receiver plane that is no wider than L_{uni}. From Figure 6, we deduce that the width of the uniform region is

$$L_{uni} = (Z - Z_0)\cdot\frac{\lambda}{dx_{grid}}, \text{ where } Z_0 = L_x^{refl}\bigg/\left(\frac{\lambda}{dx_{grid}}\right) \quad\Rightarrow\quad L_{uni} = Z\frac{\lambda}{dx_{grid}} - L_x^{refl} \qquad (46)$$

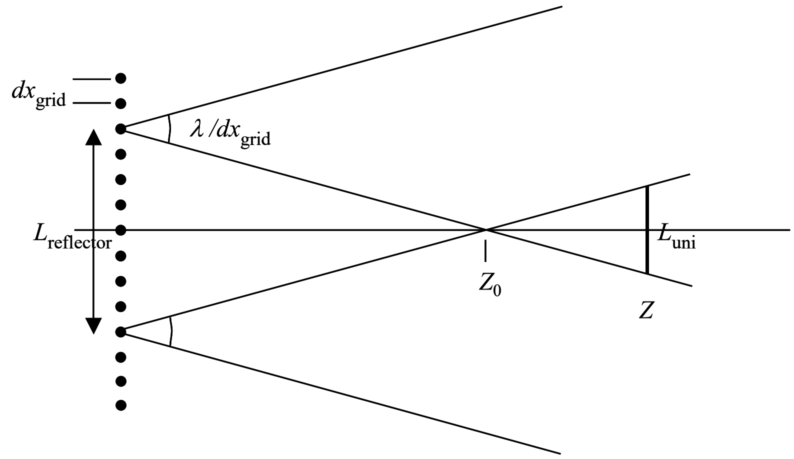

Figure 6: ROI over which average irradiance is uniform, indicated by L_{uni} in the sketch

The smallest L_{uni} occurs for the largest L_x^{refl} dimension, which is $1m$ in our test cases: in that case, $Z_0 = 14km$ and $L_{uni} = 2.57m$. We choose the ROI in the receiver plane be a square with $L_{ROI} = 1.5m$.
(ii) The second item to consider is this: if we want to compute *NIV* spatially over the receiver plane, then L_{ROI} should contain many speckles. Stated another way, L_{ROI} should contain many intensity correlation lengths. If this condition is violated, we could still compute *NIV* temporally, across many independent simulation runs, but this would much more tedious. The typical monochromatic speckle size that is expected is approximately

$$L_{x,y}^{spk} = \frac{\lambda}{L_{x,y}} Z \tag{47}$$

For our test parameter set, the two extreme situations are:

(a) At the 0-deg inclination angle, $(L_x, L_y)^{refl} = (1.0, 1.0)\,m$, and $L_{x,y}^{spk} = (0.05, 0.05)\,m$

(b) At the 80-deg inclination angle, $(L_x, L_y)^{refl} = (1.0, 0.174)\,m$, and $L_{x,y}^{spk} = (0.05, 0.29)\,m$.

Therefore, in our $1.5\,m \times 1.5\,m$ ROI, we can expect roughly 30×30 speckles for case (a), and roughly 30×5 speckles for case (b). There are actually two points to be made here. As we noted initially, computing a spatial irradiance variance over the ROI should be unbiased in the sense that the ROI spans many correlation lengths. Second, the estimation error for the irradiance variance depends on the number of independent samples, as well as on the irradiance PDF. The number of independent samples may be somewhat marginal for the 30×5 speckles case, so it is probably desirable to repeat the WaveTrain propagations for, say, 8 realizations of the rough surface and pool the irradiance data to compute *NIV*.

4.1 Comparison of theory and WaveTrain PCR simulation: results

Results for the two N_W cases are collected in Figure 7 and Figure 8. The solid red line in each figure is the theoretical curve previously plotted in Figure 3, and the symbols are PCR-simulated results for the various combinations of coherence length and plate tilt (where plate tilt controls the macro-depth of the target, as tabulated in Table 2). The horizontal-axis plot variable is $v = D_K L_z = 4\,L_z / \ell_{coh}$: according to the theory in Section 2, the *NIV* should only depend on this dimensionless ratio. Inspecting the plot for $N_w = 100$ (Figure 7), we see that the match between theory and PCR simulation is good except at the largest plate tilt of 80 deg. These results are completely consistent with the PCR parameter guidelines developed at the end of Section 3 (inequalities (44) and (45)). For example, when $\ell_{coh} = 2$ cm and $\theta = 80$ deg, inequality (45) tells us that we should have dxy < (0.35/several) cm. The actual dxy of the propagation mesh used for all runs was 1.4 cm, a gross violation of the constraint, so as expected the agreement between theory and PCR simulation is poor for this parameter combination. On the other hand, when $\ell_{coh} = 2$ cm and $\theta = 30$ deg, inequality (45) tells us that we should have dxy < (3.46/several) cm. In this case, the actual dxy=1.40 cm marginally satisfies the constraint, and indeed we see in the plot that theoretical and simulated *NIV* agree fairly well. Similar consistency checks can be made for the other data points in Figure 7 and Figure 8. The fact that the simulated results diverge from truth just when we begin to violate certain parameter constraints gives us further confidence that we correctly understand the operation of the simulation module.

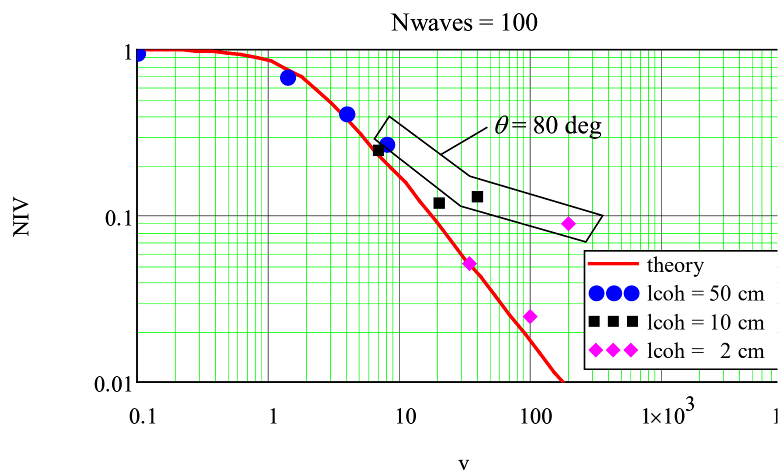

Figure 7: Theoretical and PCR-simulated results for NIV, for nWaves (N_w) = 100

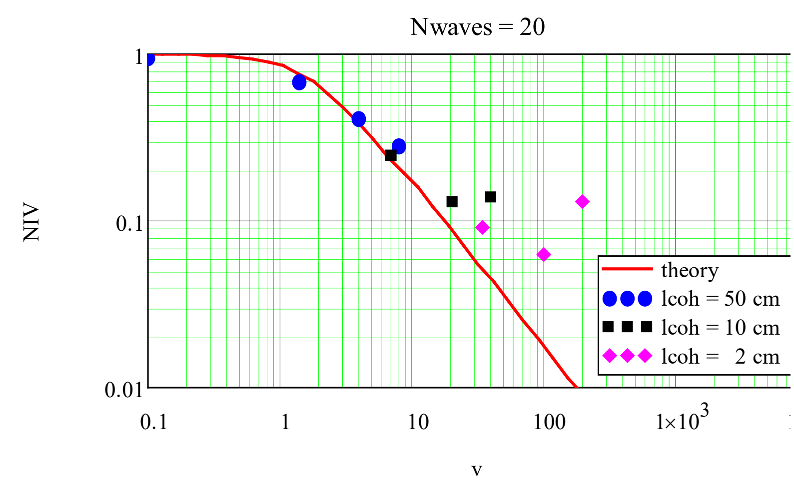

Figure 8: Theoretical and PCR-simulated results for NIV, for nWaves (N_w) = 20

5 Summary

We have carried out a quantitative test of the WaveTrain module "PartiallyCoherentReflector" (PCR). This rather complex module simulates the reflection of partially coherent illumination from an optically-rough reflector. For an analytically tractable geometry, we developed a theoretical formula for the normalized irradiance variance (*NIV*) expected at a receiver plane after scattering from the rough surface. We then simulated scattering from that geometry using the WaveTrain PCR. Over the tested range of *NIV*, we found good agreement between theory and WaveTrain simulation, when validity constraints on the simulation parameters were satisfied.